Scientific Research Publishing

Journal of Computer and Communications, 2026, 14(4), 211-237
https://www.scirp.org/journal/jcc
ISSN Online: 2327-5227
ISSN Print: 2327-5219

Prediction of Time Series Rain-Induced Attenuation Using SARIMA and LSTM Models over Subtropical Climate: A Comparison

Adewumi Oluwatoyin Ayo[1], Pius Adewale Owolawi[1], Joseph Sunday Ojo[2]

[1]Computer Systems Engineering, Tshwane University of Technology, Pretoria, South Africa
[2]Department of Physics, Federal University of Technology Akure, Akure, Ondo State, Nigeria
Email: hardewumiayour@gmail.com, owolawiPA@tut.ac.za, ojojs_74@futa.edu.ng

How to cite this paper: Ayo, A.O., Owolawi, P.A. and Ojo, J.S. (2026) Prediction of Time Series Rain-Induced Attenuation Using SARIMA and LSTM Models over Subtropical Climate: A Comparison. *Journal of Computer and Communications*, **14**, 211-237.
https://doi.org/10.4236/jcc.2026.144011

Received: March 16, 2026
Accepted: April 26, 2026
Published: April 29, 2026

Abstract

Rain fading affects terrestrial and satellite communication networks operating in higher frequencies (Ku and above), leading to signal absorption and dispersion. Rain-induced attenuation prediction is therefore vital to achieving good signal quality at both terrestrial and satellite links. The magnitude and extent of signal attenuation or loss are the primary factors to consider when planning and designing terrestrial and satellite communication links. The proposed method can anticipate datasets, whether linear or non-linear, for a temporal series of yearly attenuation patterns, modelling, and prediction in subtropical locations. The research utilizes the Long-Short-Term Memory (LSTM) method of artificial neural networks and Seasonal Auto Regressive Integrated Moving Average (SARIMA) to forecast future attenuation series after generating rain-induced attenuation using the Synthetic Storm Technique. Thirty-year rain datasets (1994 - 2023) were sourced from the South African weather station to generate time series attenuation. Three performance metric measures were used to evaluate the predictive ability of the SARIMA model with the LSTM: Mean Absolute Error (MAE), Mean Absolute Percentage Error (MAPE), and Root Mean Squared Error (RMSE). The results show that SARIMA was better at predicting rain-induced attenuation in subtropical areas than LSTM. This is because it had lower forecast performance error indicators (RMSE 1.42). The results will find their application in the digital transformation of global networks for planning 5G networks and beyond.

Keywords

Rain Attenuation, SARIMA Model, LSTM, Signal Attenuation, Auto Correlation Function (ACF), Time Series Analysis, Akaike Information Criterion (AIC), Artificial Neural Networks (ANN), Partial Autocorrelation Function (PACF)

1. Introduction

The phenomenon known as "rain attenuation" describes how rain weakens radio signals as they travel through the sky. Raindrops' absorption and scattering of the radio signal are the major phenomena influencing signal impairment. In most cases, too, signal attenuation is influenced by its frequency, the size of the drops of rain, and the volume of precipitation. In addition, heavy rainfall causes more attenuation than lighter rainfall because higher-frequency signals are more vulnerable to attenuation than lower-frequency signals [1]. Regarding satellite communication systems, rain attenuation is a critical issue since it can seriously impair signals sent from the satellite to the ground. As a result, signal propagation may be lost, data speeds may be decreased, and bigger or more potent satellite antennas may be required. Terrestrial-Satellite communication systems frequently employ strategies like frequency diversity, which involves transmitting the same signal on various frequencies, or adaptive power regulation, which modifies the signal's power depending on the degree of attenuation, to lessen the impacts of rain attenuation. In millimeter-wave telecommunication systems, rain in propagation channels reduces the performance of signals, particularly radio signals over 10 GHz, via both terrestrial and satellite paths [2]. Various approaches have been proposed to mitigate the adverse effects of rain attenuation on communication networks. These include adaptive transmission power control, frequency diversity, and dynamic link adaptation techniques. However, the effectiveness of such mitigation strategies depends largely on the availability of accurate attenuation prediction models. Predictive models, therefore, play a vital role in network planning by enabling engineers to anticipate signal degradation and design communication systems that maintain acceptable quality of service under varying atmospheric conditions [3].

Time-series analysis has proven to be an effective tool for modelling meteorological phenomena and predicting future atmospheric behavior using historical datasets. The Autoregressive Integrated Moving Average (ARIMA) model and its seasonal extension, the SARIMA model, are widely used statistical models for time-series forecasting. SARIMA models are particularly beneficial when analyzing datasets with seasonal or periodic fluctuations, such as rainfall patterns and attenuation time series. Because rainfall often follows seasonal climatic cycles, SARIMA provides a suitable framework for modelling temporal variations in rain-induced signal attenuation [4].

In recent years, advances in artificial intelligence have introduced machine learning techniques as alternative approaches for forecasting complex environmental phenomena. LSTM systems, in particular, have proven to be highly effective at modeling non-linear temporal correlations within sequential datasets. LSTM systems are a class of recurrent neural networks designed to capture long-term dependencies in time-series data through memory cells and gating mechanisms. These characteristics allow LSTM models to learn complex patterns that may not be easily captured by traditional statistical models [5].

Although both statistical and machine learning approaches have been widely applied to forecasting environmental and atmospheric variables, their relative performance varies with the characteristics of the dataset and the geographic region under consideration. For instance, several studies have applied artificial neural networks and time-series models to predict rainfall patterns and attenuation effects in different climatic environments. Nevertheless, the effectiveness of these approaches in subtropical regions such as South Africa remains an important area of investigation, particularly for high-frequency communication systems where rainfall can significantly affect signal propagation [6].

The literature [7] uses rain rate and % of exceedance as input data to train machine learning artificial neural networks (ANNs) to anticipate rain-induced attenuation on higher bands on terrestrial and satellite connections in South Africa. It is also essential for estimating cost and predicting short and long-term performance of connection paths, which is crucial in the construction of dependable networks. [6] presented the use of ANNs as a method for assessing rain-induced attenuation via terrestrial-satellite connections at a higher frequency in South Africa. [4] compared the ARIMA and SARIMA models in a subtropical site to ascertain the attenuation of the signal by rain and make real-time forecasts of the attenuation of the rain signal to be applied to microwave, terrestrial, and satellite communication systems. The conclusions of the study showed that SARIMA was superior to ARIMA in predicting the attenuation due to rainfall in South Africa since it produced better results in its error measures.

Many methods have been applied to predict such events, such as numerical and machine-learning methods using historical time series and radar system information [8]. Today, the most widely used technique for forecasting rain attenuation is obtained and evaluated using radar image data from many sources, with a large body of quantitative research frequently used in forecasting attenuation [9]. The Box and Jenkins model [10]. One methodology that stands out for its effectiveness is ARIMA, which is generally acknowledged as one of the best approaches for evaluating time series data [10]. The ARIMA method can handle monthly rain attenuation time series data, but it does not support time series that involve seasonality. SARIMA has been extensively applied over the years in predicting the trend of rainfall [11], streams and lakes modelling [12], manufacturing and finances modelling [13], and water loss modelling [14], and water loss modelling [14]. Its fascination has attracted researchers' interest in its strategy, owing to its distinctive features. It simplifies the forecasting process in that it enables researchers to use only one variable, a time series of data, in easy scenarios, but also in many more complex scenarios. A time series forecasting SARIMA model that will be used to forecast rains will need to be developed and assessed to effectively recognize signal attenuation caused by rains, limit the impact of attenuation, and allow network organizations to take the necessary actions ahead, and this will contribute towards enhancing the reliability of the broadband networks. [15] reported that different forecasting models must be used, examined, and compared in various geographic locations to enhance per-

formance for locations under consideration. In making important decisions and executing strategic planning, attenuation forecasting is required to manage signal and aquatic difficulties successfully, for instance, landslides, loss of signal, quality of service (QoS), and extreme temperatures, amongst other concerns. There should also be the ability to objectively predict and estimate attenuation [16]. A time-series model used for future forecasting is the SARIMA model. Because it is based on a historical precipitation datum across time, the time series's stochastic, seasonal, and periodic variables can be investigated [12]. [17] utilized the rainfall dataset in Dhaka city from 2000 to 2014 for their study on LSTM, Neural Network, and they achieved 76% accuracy in the LSTM model performance.

This model employs the LSTM methodology for data training; however, testing data indicates that the LSTM neural network yields significant outcomes with high accuracy compared to other weather prediction methods. The data collected from November 2007 to October 2017, at the National Climate Data Center (NCDC), provided a historical weather dataset, and the dataset includes a variety of meteorological characteristics, including pressure, temperature, humidity, and dew point [18]. LSTM networks were used [19] to efficiently capture non-linear traffic dynamics [19] by comparing his study to the existing literature, it was an intriguing possibility to show that the LSTM networks were made up of three layers, with the hidden layer made up of memory blocks, and, with the right training technique, the LSTM networks could determine the ideal time delays.

Research also indicates that the LSTM recurrent neural network on cloud data center workload forecasting models has produced empirical findings that suggest that the approach reduces the average squared errors by up to 3.17×10^3, resulting in good prediction accuracy [20].

Since both approaches may resolve issues for both linear and non-linear data sets, we employ both models in this work. The objectives of the study are to make comparisons between SARIMA and LSTM models and to use the best model to find out the rain-induced attenuation and to make monthly rain attenuation time series predictions, based on information of the applications to wireless terrestrial and satellite transmission systems. Moreover, the hybrid model combination will be compared with either of the approaches in the current study. The most suitable model among all the stations that are considered in this study is the SARIMA model $(0, 1, 0)\ (0, 1, 1)_{(12)}$.

Moreover, the results of this research can aid the Ku and Ka spectrum networks users in determining an effective way to measure and alleviate rain attenuation for better radiocommunication systems, the Internet of Things, natural disasters, and transport network control.

2. Materials and Methods

2.1. Research Location

In this research, **Figure 1** provides a topographic map of South Africa (SA), the most relevant provinces, and places where data collection took place [21].

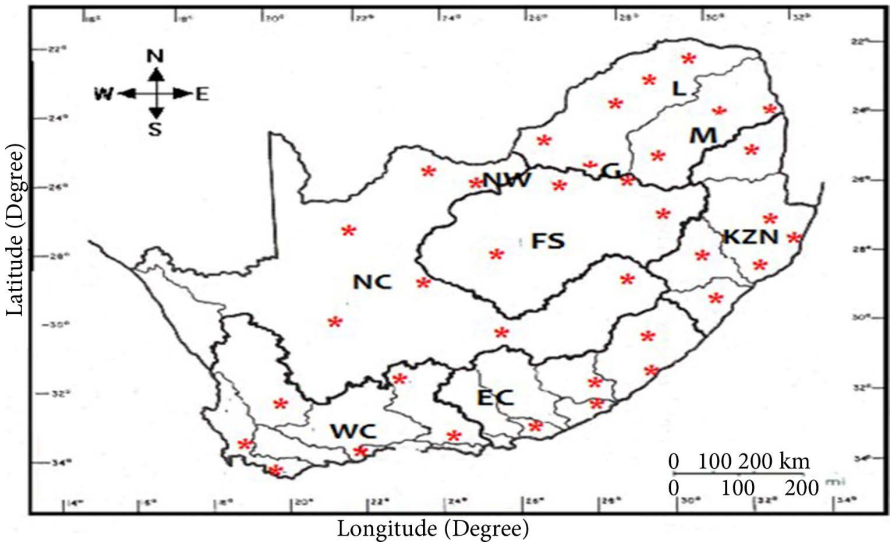

Figure 1. Shows a map of SA with the areas and sites where the data were gathered [21].

As seen in **Figure 2**, the transmission power of a microwave will be reduced as it passes through a rainy environment due to the dispersion and absorption by raindrops [22] [23]. This type of millimeter wave attenuation is referred to in [24] as rain-induced attenuation, which is defined as the relative loss of power per unit channel length, or specific attenuation, or k (dB/km). According to ITU-R P.838-4 [16], the relationship between the specific attenuation k and the rain rate, represented by R (mm/h), is as follows:

$$k = aR^b \tag{1}$$

Raindrop size distribution (DSD), polarization, and the frequency of terrestrial and satellite signals all affect the coefficients a and b in this case. Terrestrial and satellite connection attenuation can also be caused by non-rain variables such as air attenuation, the multipath effect, and free space route loss, in addition to rain-induced attenuation [22]. Thus, one can only calculate the rain-induced attenuation by subtracting the non-rain-attenuation-caused attenuation from the total attenuation. Due to its path-integrated measure, high spatial density, low implementation cost, true reflection of near-surface precipitation, and reduced human intervention, commercial microwave link (CML)-based attenuation measurement can effectively substitute or enhance more traditional rain attenuation measurement methods, such as satellites, rain gauges, and weather radars [22]. Furthermore, in addition to attenuation, CML-based measurements may estimate solid particles, fog, snow, sleet, hail, water vapor, and other phenomena [25]-[28].

2.2. Data Collection

Rainfall data were obtained from the South African Weather Service (SAWS) for six locations: Bloemfontein, Durban, East London, Nelspruit, Polokwane, and Pretoria. The dataset spans a period of 30 years (1994 - 2023) with monthly temporal resolution, resulting in approximately 360 observations per station. The rain

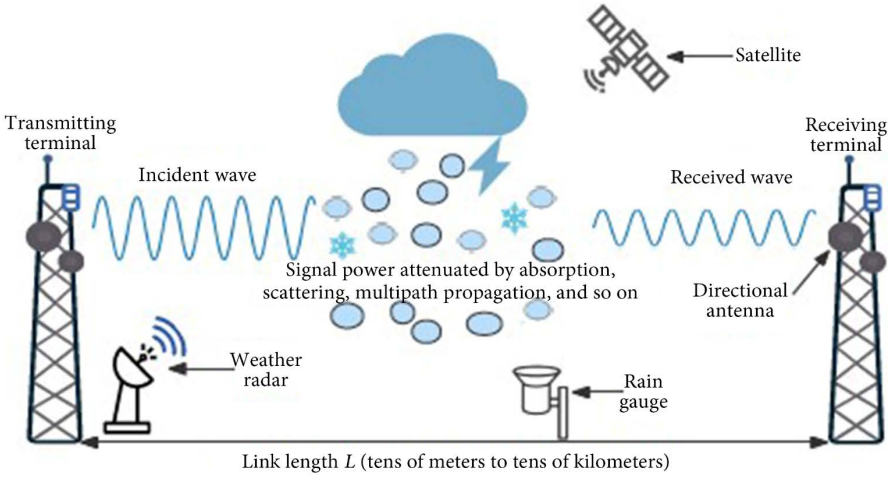

Figure 2. Basic operating principle of Commercial Microwave Links based on rainfall measurement [22].

rate data (mm/h) were converted into rain-induced attenuation (dB) utilizing the Synthetic Storm Technique (SST), which models the relationship between rainfall intensity and signal attenuation along the propagation path. The resulting attenuation time series were used as inputs for both SARIMA and LSTM models. Before modelling, the dataset was cleaned to remove missing values and normalized utilizing Min-Max scaling to enhance model convergence. To avoid an unbiased model evaluation, the dataset was divided into three subunits: Training unit: January 1994 to December 2020, Validation unit: January 2021 to December 2022, Test unit: January 2023 to December 2023. This separation prevents data leakage and ensures that model evaluation is performed on unseen data.

2.3. Analysis of Data

The dataset was divided into three segments to ensure unbiased model evaluation. Data from January 1994 to December 2020 were used for training, while data from January 2021 to December 2022 were used for validation and hyperparameter tuning. The final evaluation was performed using the test dataset from January 2023 to December 2023. This separation ensures that the test data were not used during model training or validation. Three indices are being used as the metrics to assess the models' performance. The forecast and real values are compared utilizing the root mean square error (RMSE).

$$\mathrm{RMSE} = \sqrt{\frac{\sum_{i-1}^{n}\left[Z_m - \bar{Z}_p\right]^2}{n}} \tag{2}$$

Secondly, the performance measures mean absolute error (MAE) and mean absolute percentage error (MAPE) were also used. The MAE and MAPE are represented as:

$$\mathrm{MAE} = \sum_{i-1}^{n} \frac{\left[Z_m - \bar{Z}_p\right]}{n} \tag{3}$$

$$\text{MAPE} = \frac{1}{n}\sum_{t=1}^{n}\left|\frac{Z_m - \overline{Z}_p}{Z_M}\right| \tag{4}$$

where Z_m and $\tilde{Z}_p$ are the actual and forecast values of output rain attenuation, where n is the observation number and $\tilde{Z}_p$ is the mean value. Akaike (1974) adopted a model utilizing Kullback-Leibler information for selecting a model, which Burnham and Anderson cited in [29]. They established a relationship between the highest probability and the Kullback-Leibler information for estimation, and the method was used in many statistical investigations. In simple terms, he devised AIC as a criterion for estimating Kullback-Leibler characteristics. Conversely, AIC is the most important criterion in the choice of the best SARIMA model. The AIC is a measure of the relative efficiency of different statistical methods, and of the many values, the proposed model is the one whose value is the lowest, and which is used in the forecasting [30]. Some of the statistical evaluation tools adopted to measure the performance of the model include the MAE, MAPE, and the RMSE. It considers the simplicity of the model and its quality fit. It must be made as low as possible [31].

$$\text{AIC} = -2\left[\text{log-likelihood}\right] + 2p \tag{5}$$

where p is the number of estimated parameters included in the model (*i.e.*, the number of variables plus the intercept). By displaying the model's log probability given the data, statistical output provides a straightforward method for determining how well the model fits the data overall (lower values indicate a worse fit).

2.4. Pre-Processing of Data

Before being fed into the time series model, the input data must be prepared. The following steps are often used to do this. Standardization helps put the input data on a scale that is easier to compare. The Python software command makes sure that the inputs are all in the range of (−1, 1) [32]. This pre-processing step helps the modelling process by making all inputs the same, which makes it easy to compare them. Normalizing a vector means making its mean zero and its variance one, which is another way to change the scale of the inputs.

2.5. Visualization

A brief exploratory study ought to be conducted soon before the definition of the model. To begin with, one should verify the data to ensure that it is comprehensive and correct. Check the size, type, and number of variables and check time stamp intervals; look at missing data and outliers. The second step is to determine whether the data is a trend, seasonal, or any other pattern. This will assist you in determining how to create an excellent strategy to determine whether the data is stationary or not [33]. It is more comforting to plot the autocorrelation figures to zero after some period has elapsed. This indicates that the data is consistent. When the autocorrelation gradually tends towards zero or significantly away from zero,

then the data is not stable. When the data is not stationary, it should be transformed to be in that condition. Among the most common ones are the differentiating method of mean and the adjustment of variance.

2.6. Correlogram

A correlogram is a non-moving method applied to test the accuracy of a time series with the assistance of the ACF, which results from drawing the space between *k* and *k* (lag). A population correlogram is made by graphing *k* and *k*. The only autocorrelation function we can rely on is the sample autocorrelation function since the correlation of stationary data decreases significantly with *k*. Instead, the correlogram has no zero with the non-stationary data.

2.7. Rain-Induced Attenuation Using SST

At a particular area, a rain rate time series can be converted into a signal attenuation time series using the synthetic storm (SST) method [34]. The mathematical and physical techniques illustrate a fundamental understanding of factors such as the signal's path length through the rain cell, the speed of the rain cell (v), and the rain rate (R) at the specific location being analyzed [35]. Layer A consists of raindrops at 20˚C, while Layer B comprises melting hydrometeors at 0˚C. These two layers constitute the vertical structure of the precipitation medium [36].

For Ku and Ka band signals in a subtropical region like Pretoria, South Africa, an attenuation series is used to translate observed rain rate data during a rain event into a fade duration statistic based on the SST [37].

The purpose of this study is to generate time series rain-induced attenuation because of real rain rate data at the research location, to propose mitigation methods for terrestrial and satellite communications in South Africa. The monthly rain attenuation time series data from one of the sites is utilized to validate the rain attenuation time series [38].

For analysis, the rain-induced attenuation time series results are shown graphically. The model is assessed not just on a long-term geometric basis but also on its applicability by comparing current models with monthly rain attenuation time series data.

2.8. Seasonal ARIMA Model

Time-series data is analyzed using the SARIMA model to identify both seasonal and non-seasonal components. The parameters for the autoregressive, differencing, and moving average components are written as SARIMA (p, d, q) $(P, D, Q)_s$. The plots of the ACF and PACF were used to establish the model parameters. The optimal model configuration selected for this study was SARIMA (0, 1, 0) $(0, 1, 1)_{(12)}$. The model was fitted to the training dataset and validated using the validation set. Time series analysis is effective for studying rain attenuation because the data inherently follow a chronological sequence. The researchers employed SARIMA modelling to analyze the data. Essentially, an ARIMA model explains how current

data relates to past data. The SARIMA model enhances this by integrating both seasonal patterns and regular, non-seasonal trends, providing a more comprehensive understanding of the situation.

$$\text{ARIMA}\left(p,d,q\right)\times\left(P,D,Q\right) \tag{6}$$

In this context, the variables are defined as follows: The seasonal autoregressive (AR) order is denoted by p, the non-seasonal differencing by d, the seasonal moving average (MA) order by q, and the repeated seasonal attenuation pattern's time span by S.

If differencing operations are not included, the model can be expressed more formally as:

$$\phi\left(B^s\right)\varphi\left(B\right)\left(X_t-\mu\right)=\theta\left(B^s\right)\theta\left(B\right)w_t \tag{7}$$

The element that is non-seasonal is:

$$\text{AR:}\quad \varphi\left(B\right)=1-\varphi_i B-\cdots-\varphi_p B^p \tag{8}$$

$$\text{MA:}\quad \theta\left(B\right)=1+\theta_i B+\cdots+\theta_q B^q \tag{9}$$

The seasonal element is :

$$\text{Seasonal AR:}\quad \phi\left(B^s\right)=1-\phi_i B^s-\cdots-\phi_p B^{ps} \tag{10}$$

$$\text{Seasonal MA:}\quad \theta\left(B^s\right)=1+\phi_i B^s+\cdots+\phi_q B^{qs} \tag{11}$$

2.9. Unit Root Test

The Augmented Dickey-Fuller test (ADF test) is another name for the unit root test. It is typically formulated in the following hypothesis format:

$$H_0:\rho_j=0 \tag{12}$$

and

$$H_1=\rho_j\neq 0 \tag{13}$$

At the 5% level of significance, the unit root for non-stationarity (H_0) is rejected if the probability value (p) is less than 0.05, meaning a robust indication against the null hypothesis. Consequently, the data is considered stationary. The mean and variance of the attenuation values seem to be stable. However, a stationary test using the ADF test is carried out to increase accuracy [39].

H_0: Non-stationary attenuation data;

H_1: Stationary attenuation data with a statistical test.

Accordingly, it is possible to conclude that the attenuation values are stationary, as seen in Table 1.

2.10. Choosing the Best Model

By comparing the lowest values of the ACF, Bayesian information criterion (BIC), and AIC, the best SARIMA models were selected. The AIC determines the best model, with the model with the lowest AIC value being preferred [40].

2.11. Model Identification

The key stages in time series analysis involve identifying the appropriate model and applying it to the available data. It's essential during this phase to determine the values of (p, d, q) and $(P, D, Q)_{(s)}$. The Box-Jenkins method is suitable solely for stationary time series data, with the main objective being to reduce the number of exceedingly complex models by utilizing computationally efficient algorithms to plot the data over time and identify any anomalies [41].

When carefully examining the plot, one can usually identify whether a series has a trend, seasonality, outliers, non-constant variances, or other non-normal and non-stationary occurrences, and this knowledge would aid in selecting the appropriate data transformation [41]. We should employ differencing and variance-stabilizing transformations if the variance increases with time. A logarithmic transformation is frequently required for a series with a non-constant variance. The subsequent step is to ascertain the starting values of the moving average order q, auto-regressive order p, and order of differencing d for the seasonal parameters P, D, and Q [40]. The ACF and the PACF are crucial instruments in time series analysis that help determine possible correlations between data and comprehend the structure of a time series [42]. The correlation between a time series and its lag values is measured by the ACF. As the lag increases, it illustrates the correlation between each prior observation and the present observation. The correlation between a time series and a lagged version of itself that cannot be adequately explained by intervening values is measured by PACF. In accounting for the effects of various temporal delays, it aids in distinguishing the direct relationship between observations recorded at two distinct periods. The PACF aids in identifying the order of a moving average (MA) model by analyzing the moment at which the PACF values cease [43].

The amount of linear dependence between time series data separated by a lag q is estimated by the ACF.

The number of necessary autoregressive terms (p) is determined by the PACF. The sequence in which the difference frequency changes from a non-stationary to a stationary time series is determined by parameter d.

If differencing is necessary, a linear trend will be shown on the time plot. During the placement of the initial values of D and d, the following stage involves analyzing the ACF and PACF to calculate the values of P, Q, p, and q. Statistical methods can be used to identify the parameters and the associated standard errors once the model has been essentially set up. Forecast values of a time series may be predicted using the estimated model once a model has been found and all its parameters have been established.

2.12. Long-Short Term Memory (LSTM) Model

Time series prediction and natural language processing both frequently employ the LSTM architecture, which is due to recurrent neural networks (RNNs). The flowing data that is recorded and kept in cells serves as its inspiration. Data may then be transferred from several earlier instances to the present by connecting

modules from the past. Due to the gates in each cell, the data in each cell can be rejected, filtered, or added to prepare the subsequent cells [44]. The active cells either transfer or reject input, and the gates concentrate on a neural network with sigmoidal form layers. A value between 0 and 1 is produced by each sigmoid layer, signifying the total of all data segments that must be allowed in each cell. More specifically, prediction one indicates that "let it all pass", but the predicted low value predicts that "nothing should be allowed to pass". Each LSTM contains three different kinds of gates that control a state for each cell:

i. A number between 0 and 1, where 1 indicates success, is produced by the forget gate. "fully save this", whereas 0 indicates "ignore this".

ii. The memory gate, the sigmoid layer, decides which of the cell's most recent data should be retained, followed by the tanh layer. Which values to change is decided by the "doorway layer", the first sigmoid layer. After that, a new prospective value vector is produced by the tanh layer and may be included in the state.

iii. The output gate specifies what each cell should produce. Both the newly added filtered data and the cell state will decide the final value. The general procedure is represented graphically in **Figure 3**. The following equation describes the network's mathematical definition.

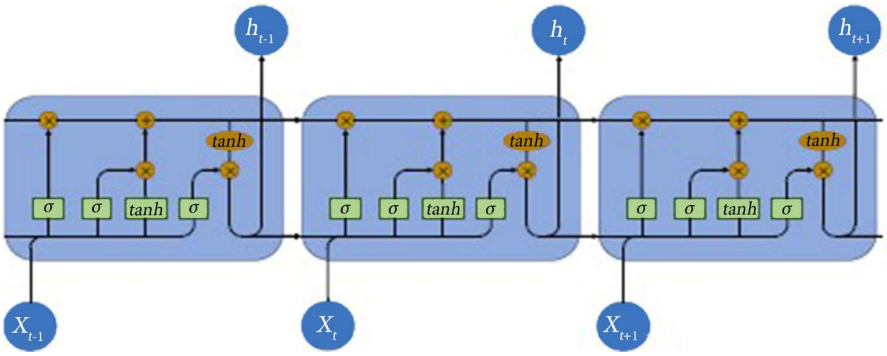

Figure 3. Four interacting layers that make up an LSTM module (/colah.github.io is the source).

$$f_t = \sigma\left[W_f\left[h_{t-1}, x_t\right] + b_f\right] \tag{14}$$

$$i_t = \sigma\left[W_i\left[h_{t-t}.x_t\right] + b_i\right] \tag{15}$$

$$\tilde{C}_t = \tanh\left[W_c\left[h_{t-1}, x_t\right] + b_c\right] \tag{16}$$

$$C_t = f_t * C_{t-1} + i_t * \tilde{C}_t \tag{17}$$

$$o_t = \sigma\left[W_o\left[h_{t-1}, x_t\right] + b_o\right] \tag{18}$$

$$h_t = o_t * \tanh\left[C_t\right] \tag{19}$$

where C_t represents the state of the unit, h_t refers to as its output, and f_t, i_t, and o_t are referred to as the forget, the input, and the exit gates, respectively. It is crucial to remember that the LSTM network functions similarly to the conventional neural network (CNN), with layers and several units per layer, and that

the mathematical formulation is for a single unit. Neural networks are known to perform well in stochastic and non-linear time series data when other approaches fall short, in contrast to the SARIMA methodology, which is well-known for its capacity to handle seasonal linear time-series prediction [45]. One issue with long-term series is that minor errors might become widespread and lead to a catastrophic failure of the model's convergence [46]. Given that LSTM Neural Networks have been demonstrated to be the most effective neural network type for time series prediction, we will employ this particular form of recurrent ANN [47]. LSTMs develop the capacity to retrieve data utilizing long-term memory cells, which may retain information that a basic NN cannot.

They can also handle decreasing gradient issues that regular recurrent neural networks have, which may affect performance. This clarifies the suitability of LSTMs for long-term series forecasting. For instance, a comparison of wind speed using ARIMA and LSTM in [48] showed the apparent advantages of LSTM, but it additionally illustrated the point that, due to the specific NN architecture's lack of training and pattern learning, the ARIMA technique may outperform LSTM for smaller datasets. To determine a configuration that was almost ideal, we performed a grid search of parameters and architectures for each of the LSTM neural networks shown in the results section. Standard momentum = 0.9 is utilized in the SGD (stochastic gradient descent) [49] optimizer, which produces superior results for some networks, while the Adam optimizer [50] is used in other cases. Assuming an average learning rate of 0.01 with an update of 0.008 and a "patience" parameter of 5, the method modifies the learning rate every eight epochs if the loss does not improve.

Some research determined that using 100 units produced better results than using the usual 40 units per layer; however, this came at the cost of a longer computation time. The accuracy we obtained was generally logical when utilizing one input layer, one hidden LSTM layer, and one dense output layer. Rectified Linear Unit (ReLU) activation functions are used in all layers since other activation functions resulted in decreased accuracy. To avoid overfitting, we combined grid search with validation error over the course of the 20 - 60 training epochs. Furthermore, a callback that employed a 5-epoch patience was employed, and the tracked signal deterioration decreased the learning rate from 0.01 by a factor of 0.08. To simulate a time series using an LSTM RNN, the input data must be suitably structured in a sliding window manner. The final LSTM model architecture consisted of one input layer, one hidden LSTM layer with 100 units using the ReLU activation function, and a fully connected dense output layer. The input data were structured using a sliding window approach with a look-back period of 12 months to predict the next time step. The dataset was normalized using Min-Max scaling before training, and an inverse transformation was applied to obtain the final predictions. The model was trained using the Adam optimizer with a learning rate of 0.01, a batch size of 32, and training epochs ranging from 20 to 60. Early stopping with a patience of 5 epochs was used to prevent overfitting. The reported results correspond to the average performance over multiple

training runs. The data provided in this research is monthly data.

Therefore, a 12-step prediction window can be used, for example. This implies that we forecast the thirteenth sample using twelve data samples, or data spanning a full year. The MAE was utilized to compare the methods and facilitate the transfer to the real-world scenario, while the MSE was selected as the loss error. A prediction was estimated for each monthly rain attenuation time series in the test set and contrasted with the monthly rain attenuation time series data, which was not utilized to train any algorithms. The mean for each monthly rain attenuation time series was first determined, and then the absolute value of their difference was calculated to achieve this. It is validated that the average monthly rain attenuation time series throughout all test days is the result presented in **Table 1**.

3. Results and Discussion

The first step in time series modeling is to visualize the dataset to check for a stationary mean and variation. If the dataset is not stationary with respect to the mean or variance, then differencing is employed; otherwise, a transformation is needed. **Figures 4(a)-(f)** present the trends of time series of rain-induced attenuation at Bloemfontein, Durban, East London, Nelspruit, Polokwane, and Pretoria, respectively. The results show that the time series has a seasonal cycle and is not stationary since the data are time series attenuation data. The ACF and PACF of the actual data, which can be seen in **Figures 5-10**, show that the attenuation data is not steady. To fit a SARIMA model, stationary data are needed for both the variance and mean. The seasonality tendency was evident in the attenuation time series data from 2023 to 2024 due to its nature. Moreover, the SARIMA model was used in this paper to predict attenuation for subsequent years. The comparative performance of SARIMA and LSTM models across the six locations reveals distinct patterns influenced by regional climatic characteristics. SARIMA demonstrates superior performance in inland regions such as Bloemfontein, Nelspruit, Polokwane, and Pretoria. These locations exhibit relatively stable and seasonal rainfall patterns, which are effectively captured by the linear and seasonal structure of the SARIMA model.

In contrast, the LSTM model outperforms SARIMA in coastal regions, particularly Durban and East London. These regions are characterized by higher rainfall variability and complex atmospheric interactions influenced by oceanic conditions. The ability of LSTM to model non-linear dependencies enables it to better capture these dynamics.

Furthermore, model performance varies across different months. Both models show improved accuracy during low-attenuation periods, while performance decreases during high-attenuation months such as March to April and October to November. This indicates the challenge of predicting extreme attenuation events. An important observation is the underestimation of peak attenuation values, where measured attenuation (~8 dB) exceeds predicted values (2 - 5 dB). This discrepancy is primarily attributed to normalization and smoothing effects during pre-processing, which tend to suppress extreme values. This limitation suggests

the need for improved scaling techniques or hybrid modelling approaches for better peak prediction.

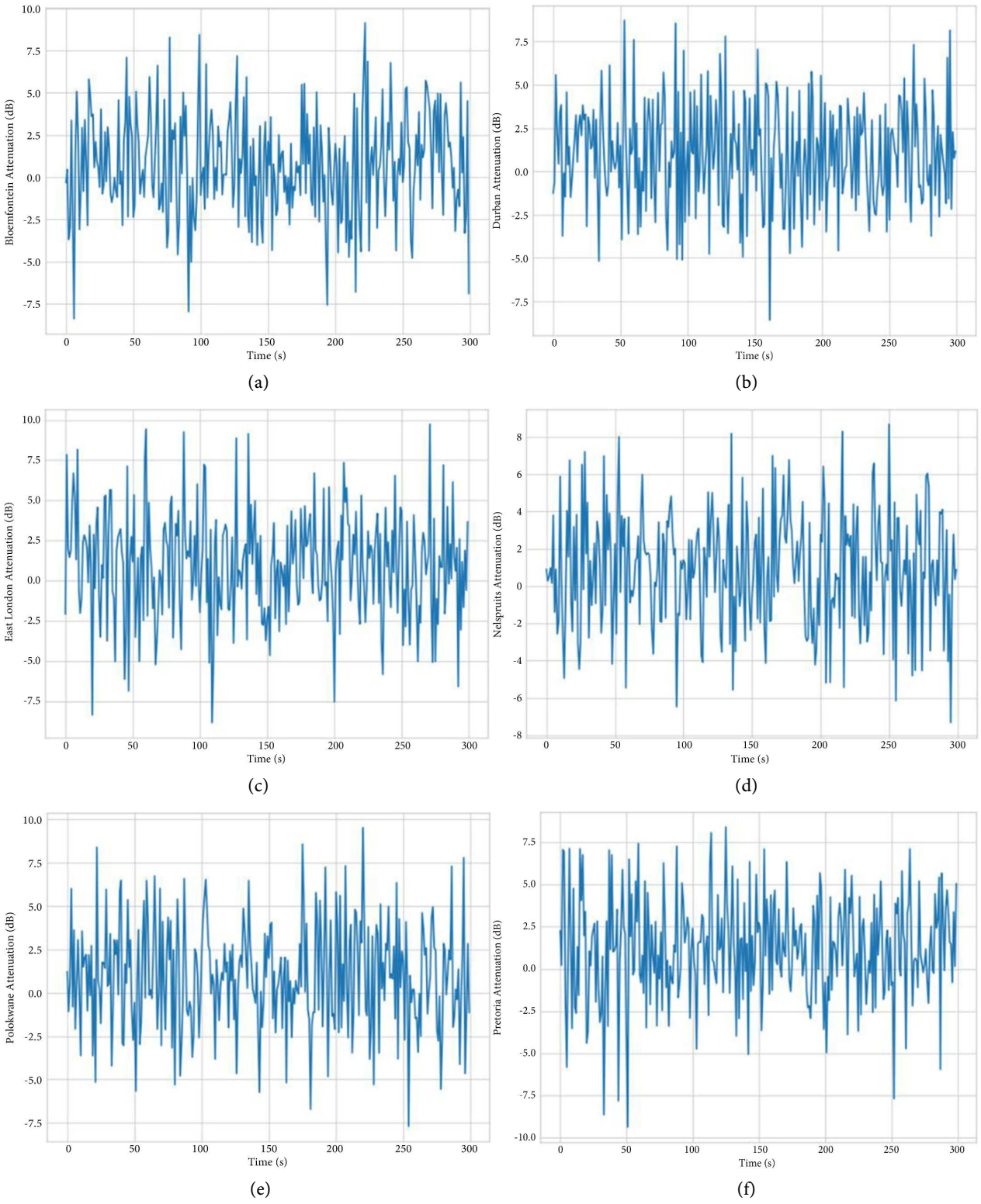

Figure 4. Trends of time series of rain-induced attenuation at (a) Bloemfontein, (b) Durban, (c) East London, (d) Nelspruit, (e) Polokwane, and (f) Pretoria.

Figures 4(a)-(f) show a change in the monthly rain attenuation time series and a reduction in attenuation strength. Nelspruit experiences the most attenuation for roughly 60 seconds, or 8.2 dB, whereas Durban and Pretoria experience the lowest attenuation (Figure 4(b) and Figure 4(f)). The average attenuation between 2003 and 2024 was 8.5 dB, with a 0.1 standard deviation. The attenuation data are steady in terms of their mean and variance, as can be seen by looking at Figure 4(a)-(f). The ADF model is utilized for stationary data analysis.

ACF and PACF Identification:

The ACF is used to measure the correlation between a time series and the lagged values. Important time-dependent trends are identified, and they help in establishing the impact of past values on future values [51]. The PACF computes the correlation between the time series and its lagged values after taking the effect of intermediate delays into consideration. It is employed in SARIMA models to ascertain the autoregressive (AR) component's order to determine if SARIMA models have an MA component [52]. It helps determine the optimal number of lag observations (p) in SARIMA models. ACF and PACF must be employed to choose the optimum time-series models for predicting rain attenuation. They help determine if a deep learning technique (LSTM) or a standard statistical approach (SARIMA) is more suitable for certain locations based on their climatic factors. When the data is stable, it is ready for identification to produce the SARIMA model forecast (p, d, q) $(P, D, Q)_{(12)}$. The attenuation statistics, ACF and PACF, are shown to help identify them. Figures 5-10 display rain attenuation data for ACF and PACF figures in Durban, Pretoria, Polokwane, Bloemfontein, East London, and Nelspruit, accordingly.

Prediction of SARIMA and LSTM Models:

We examine SARIMA and LSTM models within several frameworks. The evaluation of their performance metrics can be seen in Table 1.

Table 1. Evaluation of RMSE, MAPE, and MAE based on the SARIMA and LSTM models.

SARIMA Stations	SARIMA Metric Performance			LSTM Metric Performance		
	RMSE	MAPE	MAE	RMSE	MAPE	MAE
Bloemfontein	1.570	59.13	1.34	4.042	100.04	2.07
Durban	1.80	80.95	1.63	1.63	47.72	0.88
Nelspruit	1.54	70.49	1.42	3.13	55.82	1.36
Polokwane	1.79	70.21	1.56	4.41	99.43	2.26
Pretoria	1.42	48.72	1.16	2.03	57.08	1.30
East London	1.75	62.53	1.45	1.21	15.82	0.48

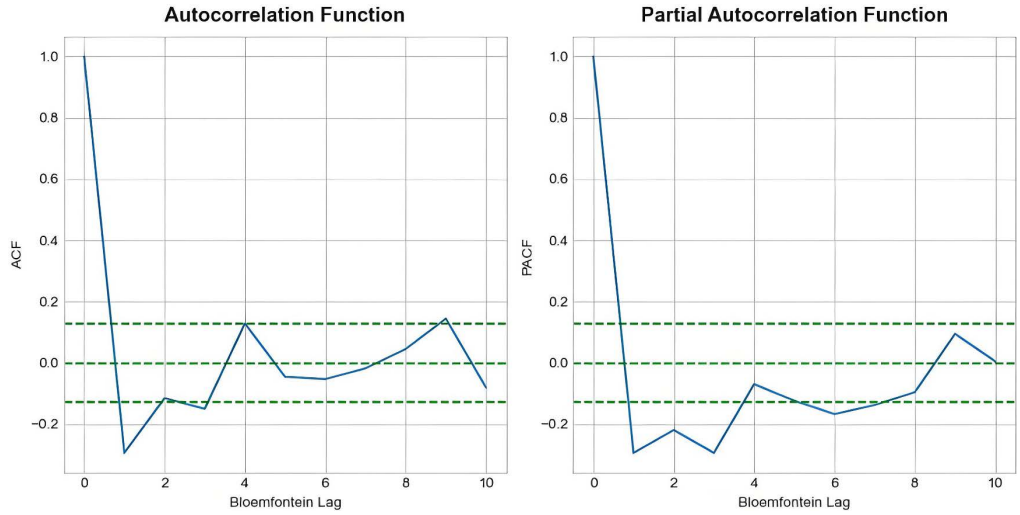

Figure 5. Bloemfontein's ACF and PACF trends.

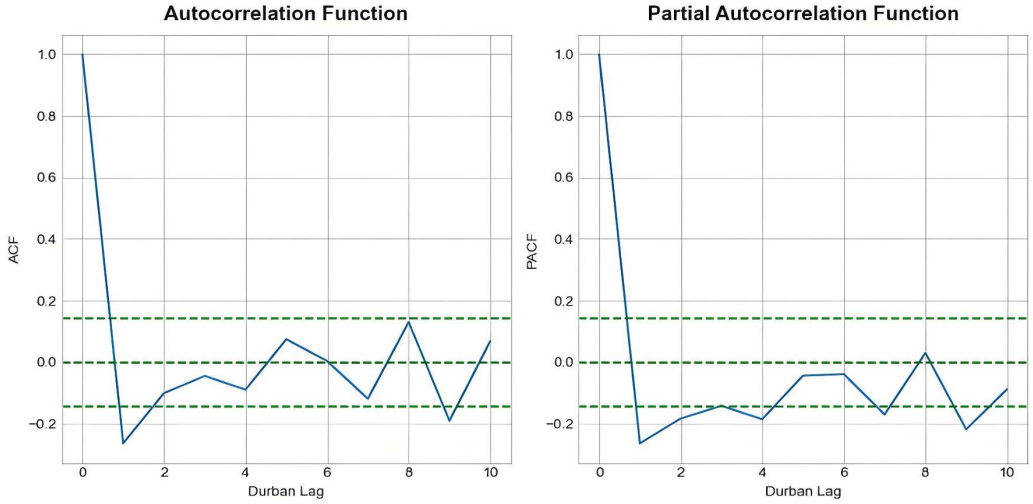

Figure 6. Durban's ACF and PACF trends.

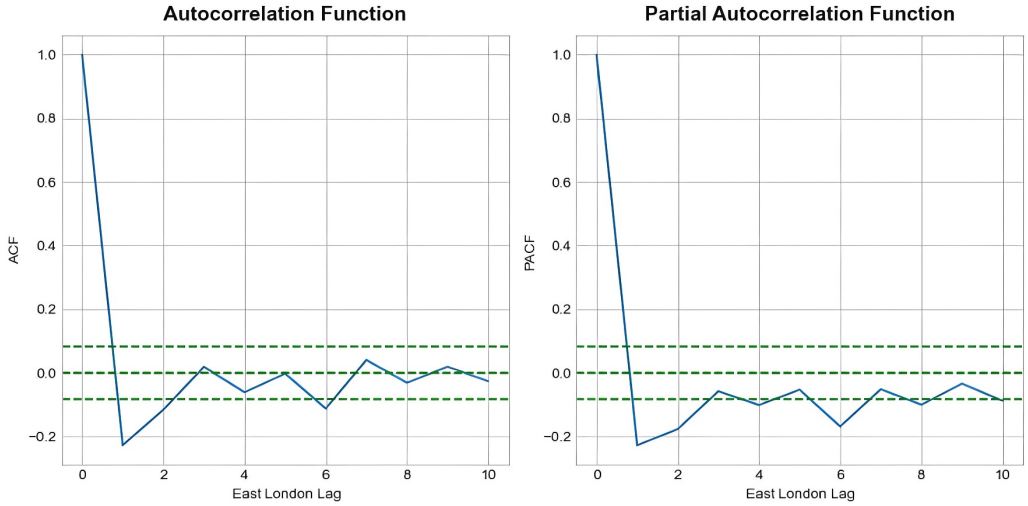

Figure 7. East London's ACF and PACF trends.

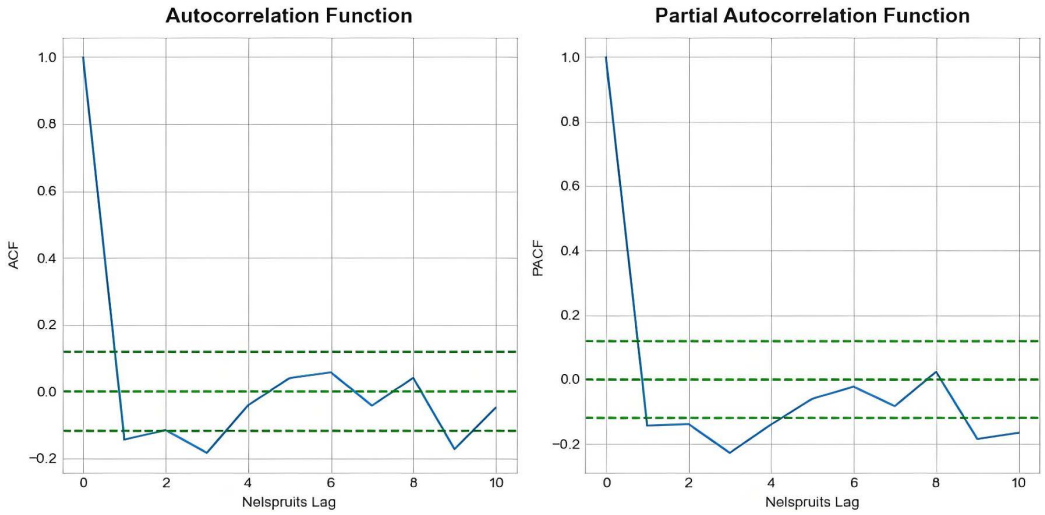

Figure 8. Nelspruit's ACF and PACF trends.

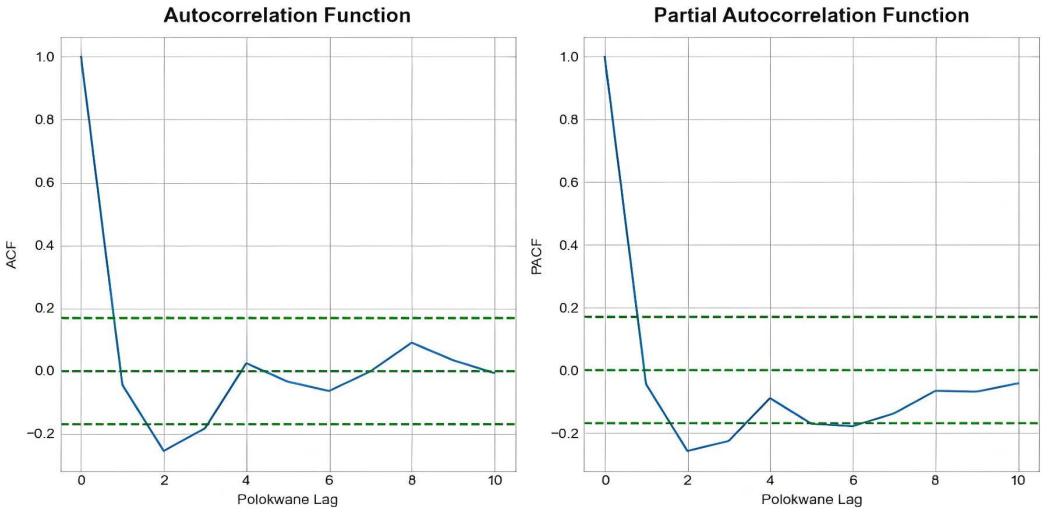

Figure 9. Polokwane's ACF and PACF trends.

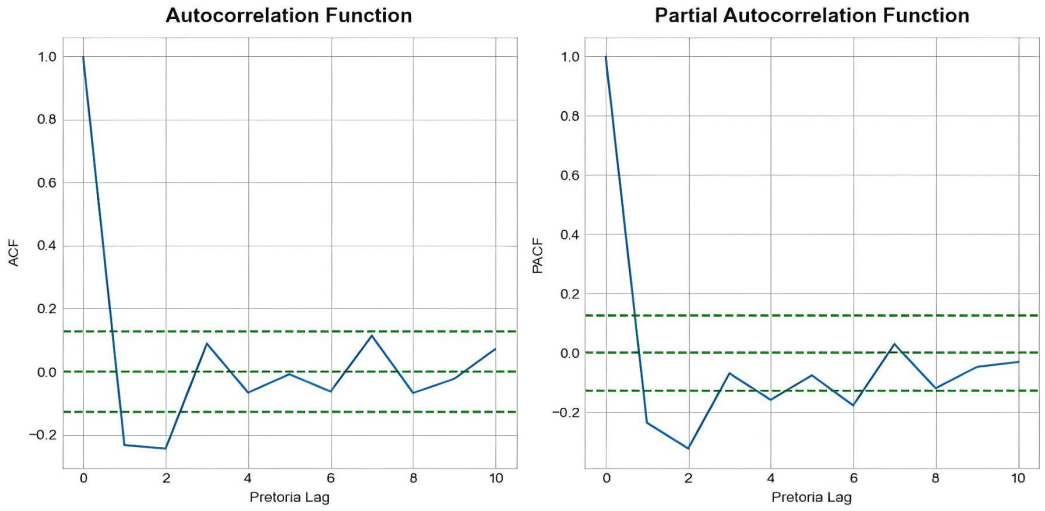

Figure 10. Pretoria's ACF and PACF trends.

4. Prognostication

Time series analysis's main objective is to predict future values [53]. Once we select the best model, we prepare it for prediction. The goal of the forecasting method is to boost confidence in the future prediction of the data; meanwhile, the decrease in reception for each research location was found to follow the same trend, suggesting that attenuation will happen at different places throughout South Africa within the same time of signal transmission. The time series plot and correlogram of the series were analyzed to determine the presence of non-stationarity, seasonality, and trend [54]. It is evident from the figures that the time series plot exhibits wave-like patterns, and **Figure 4(a)-(f)** shows that there are seasonal elements in the signal time series, which proves the sinusoidal wave-like shape on ACF plots in **Figures 5-10**.

Additionally, it can be inferred from **Figures 5-10** that there were no apparent fluctuations in the series' mean or variance across the time span covered for this investigation. The PACF plots in **Figures 5-10** show significant rises during the first two seasonal lags (Lags 2 - 10, where lags are expressed in months). **Figures 5-10** also display large increases in the non-seasonal lags from ACF plots, with one notable spike occurring at the first seasonal lag (Lag 7). The seasonally differenced series' correlogram indicates that SARIMA (0, 1, 0) (0, 1, 1) $_{(12)}$ would be a suitable model for time series attenuation. The model with the lowest values of the specified criteria is the best one.

Figures 11 through 16 clearly demonstrate the SARIMA, LSTM attenuation forecasting, residual, seasonality, and trend snap around zero to 0.10, as well as the consistent variance across time. The ACF and PACF plots in **Figures 5-10** also show that every spike, except Bloemfontein and East London, is within boundaries, indicating that none of them are significant and, thus, not autocorrelated. The efficacy of the fitted LSTM and SARIMA models in predicting rain-induced attenuation of the stations in question is then shown using actual and forecast performance measure graphs in **Figures 11-16** and **Table 1**. To evaluate the forecast performance of the two approaches, we first look at their performance metrics. **Table 1** illustrates that the values forecasted by the fitted SARIMA model are more accurate than those of the LSTM model at more time points. **Figures 11-16**, March to April and October to November appear to experience higher attenuation, and these months likely coincide with rainy seasons or periods of high atmospheric conditions in the location under consideration. As a result, when designing or operating communication systems in Bloemfontein, Durban, East London, Nelspruit, Polokwane, and Pretoria, there must be a plan for higher attenuation in specific months, such as March to April and October to November.

From the sequential data of March-April 2023 to October-November 2024, the trend of the plots presented in **Figure 11** and **Figure 16** shows the period during which we have signal loss during the months of the year. We can clearly see that there is fluctuation in the signal because of rain-induced attenuation during the months of March-April to October-November. The measured data were found to

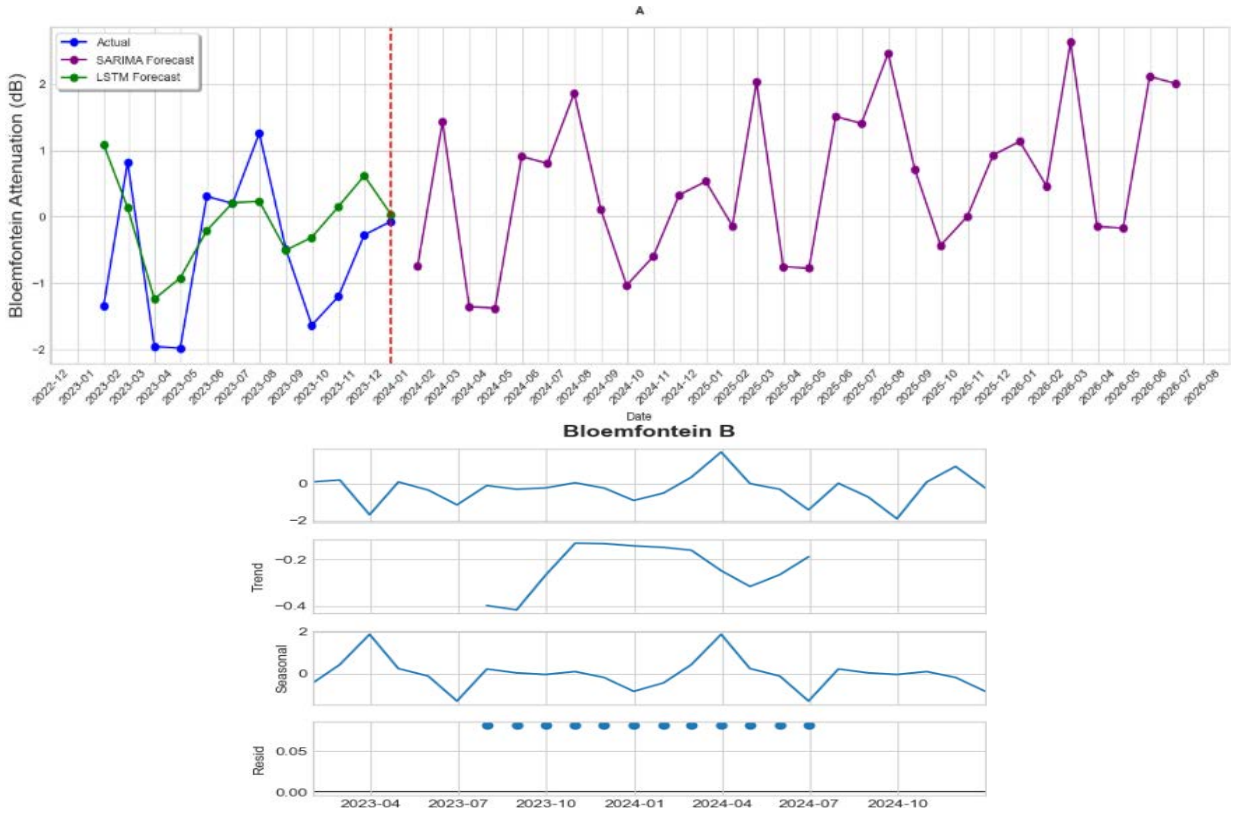

Figure 11. Bloemfontein SARIMA, LSTM attenuation forecast, and the SARIMA seasonal series.

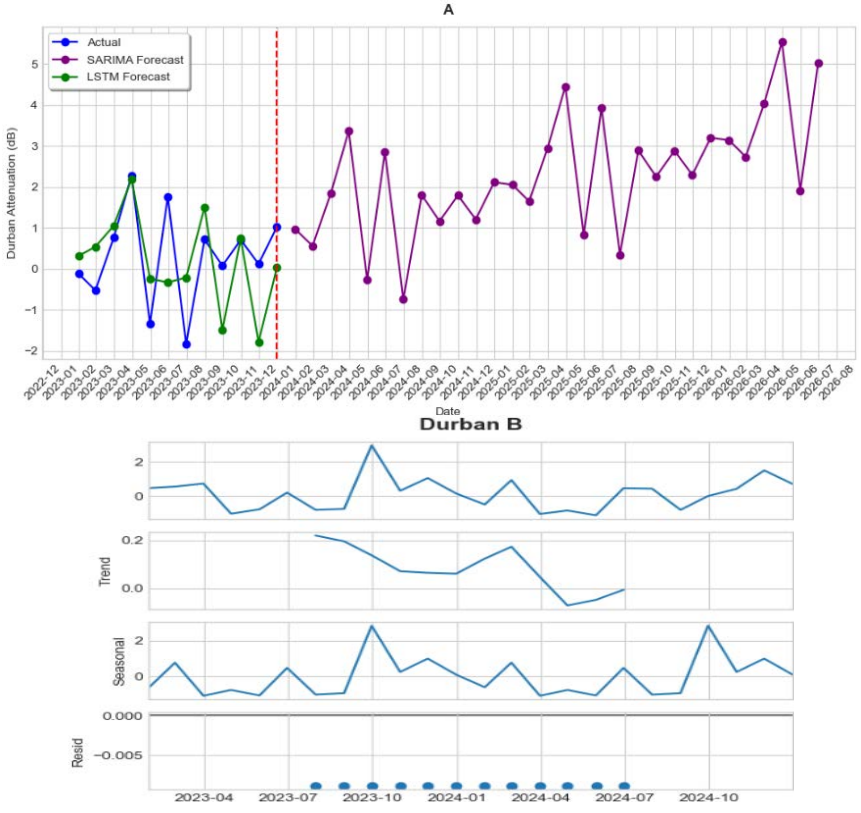

Figure 12. Durban SARIMA, LSTM attenuation forecast, and the SARIMA seasonal series.

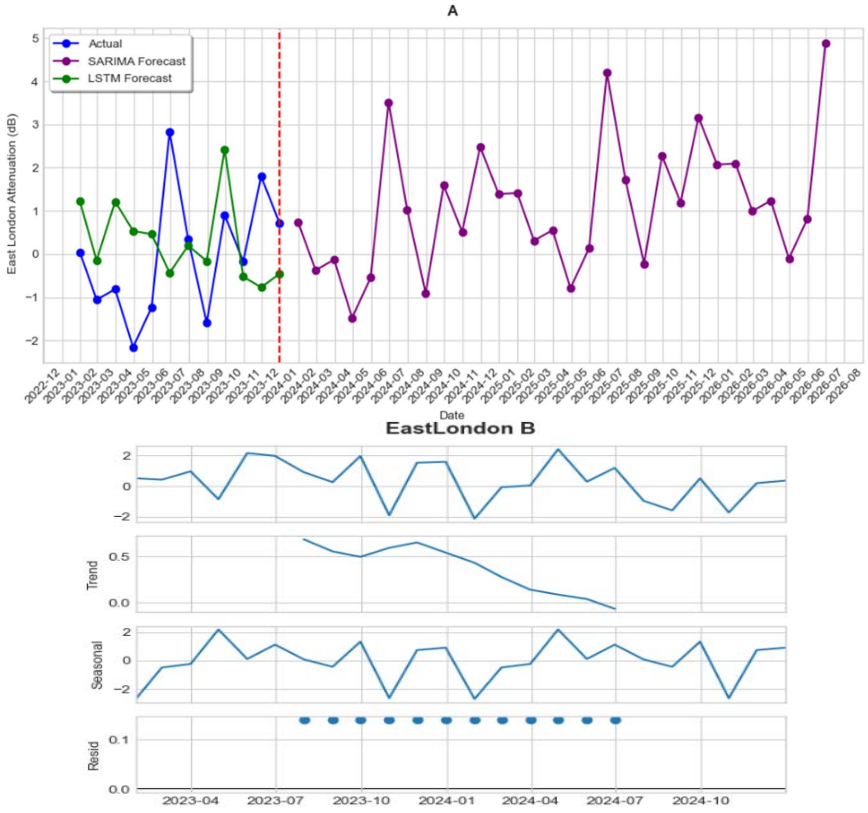

Figure 13. East London SARIMA, LSTM attenuation forecast, and the SARIMA seasonal series.

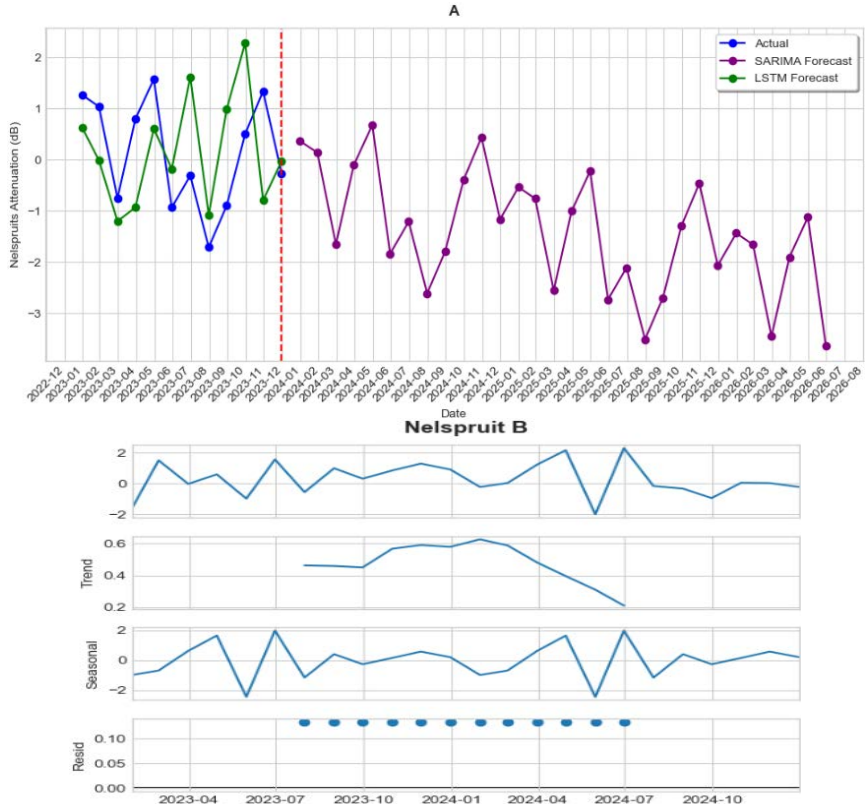

Figure 14. Nelspruit SARIMA, LSTM attenuation forecast, and the SARIMA seasonal series.

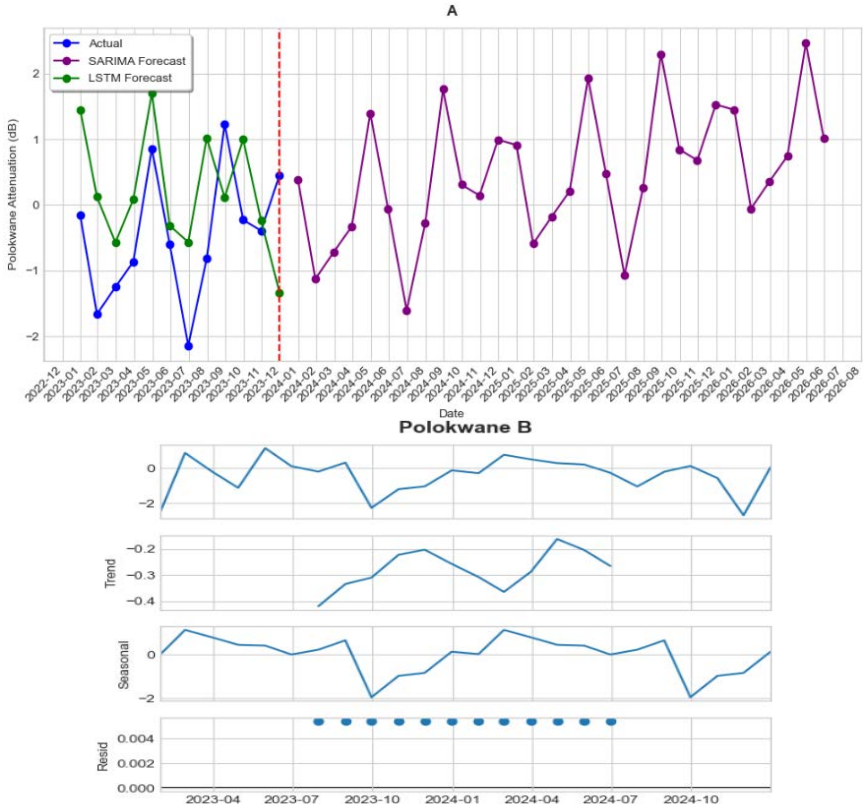

Figure 15. Polokwane SARIMA, LSTM attenuation forecast, and the SARIMA seasonal series.

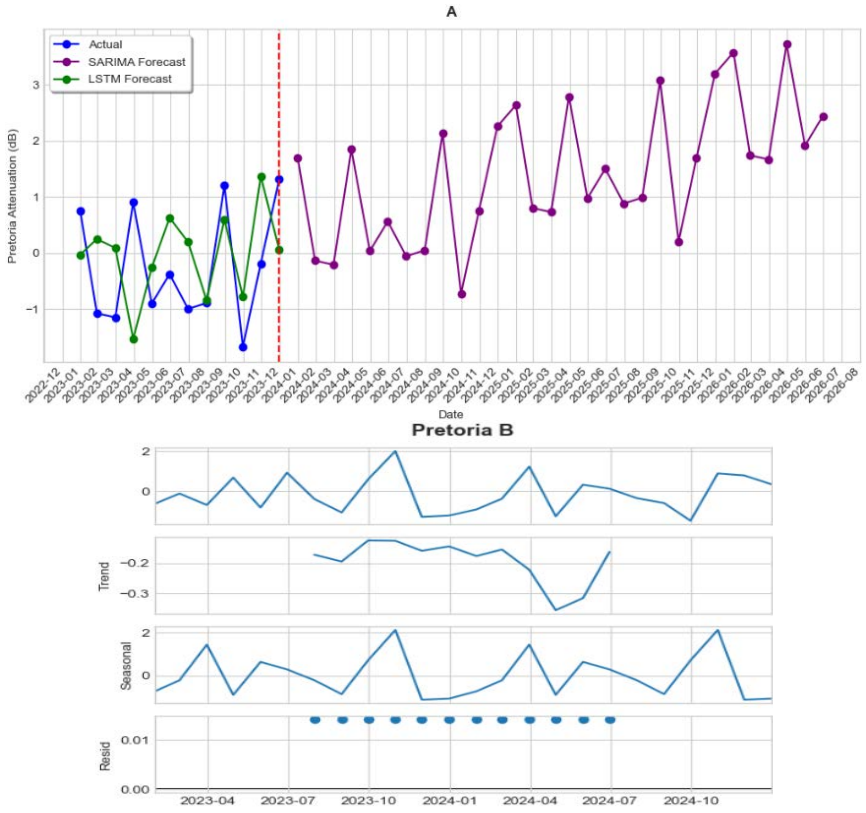

Figure 16. Pretoria SARIMA, LSTM attenuation forecast, and the SARIMA seasonal series.

be around 8 dB, while the predicted attenuation ranges from about 2 to 5 dB. The observed underestimation of peak attenuation values (measured ~8 dB versus predicted 2 - 5 dB) can be attributed to the normalization and smoothing effects introduced during data pre-processing, particularly Min-Max scaling. While normalization improves model convergence, it may suppress extreme values if not properly inverse-transformed. This limitation highlights the need for improved scaling techniques or the incorporation of extreme value modelling to better capture peak attenuation events, which are critical for communication system design. Table 2 clearly shows the best model per station.

Table 2. Model comparison table.

Stations	Best Model
Bloemfotein	SARIMA
Durban	LSTM
Nelspruit	SARIMA
Polokwane	SARIMA
Pretoria	SARIMA
East London	LSTM

5. Conclusions

The SARIMA and LSTM models for forecasting monthly rain-induced attenuation in South Africa's subtropical areas were compared in this study. The results demonstrate that SARIMA provides better performance in inland regions characterized by stable and seasonal rainfall patterns, while LSTM is more effective in coastal regions with higher variability and non-linear dynamics. The findings highlight the significance of choosing predictive models because of regional climatic characteristics rather than adopting a single universal approach. Additionally, the observed underestimation of peak attenuation values indicates the need for improved modelling techniques capable of capturing extreme events. Generally, this research will lead to more credible attenuation prediction techniques, which are required in the design and optimization of high-frequency terrestrial and satellite communication systems.

The study has effectively evaluated the forecast performance of LSTM and SARIMA when it comes to estimating the rain attenuation of the studied stations in South Africa, using correlation analysis and performance measures to show the significant difference. Even while SARIMA has the lowest forecast error, the correlation index suggests that there is no discernible difference between the two approaches' prediction values, and the performance metrics support these. As a result, they can be employed successfully to offset the predicted signal loss in the South African province. After the signatures of a set of various models were tested, the findings show that SARIMA tends to work better than LSTM in inland areas like Bloemfontein, Nelspruit, Polokwane, and Pretoria. However, LSTM demon-

strates superior performance in coastal regions such as Durban and East London, where rainfall patterns exhibit higher variability and non-linear characteristics. This suggests that statistical models perform better in stable climatic regions, while deep learning models are more suitable for complex and highly dynamic environments. For subtropical terrestrial-to-satellite communication systems, the model could be used to determine the optimal planning time to reduce the impact of signal attenuation. These predictions can aid in developing climate-resilient communication infrastructure by identifying potential periods of significant signal degradation in communication systems. A limitation of the research lies in the infrastructure for collecting the data. In the future, hybrid models will be developed to examine, compare, and investigate the phenomena of signal loss in South Africa.

Acknowledgements

The authors would like to extend their sincere gratitude to Tshwane University of Technology in Pretoria, South Africa, as well as to the SAWS for supplying the data used in this study.

Conflicts of Interest

The authors declare no conflicts of interest regarding the publication of this paper.

References

[1] Basarudin, H., Mohd Yunus, N.H., Hasan, N., Aminudin, N.A.I., Ramli, A.F., Chung, B.K., *et al.* (2024) Rain Fade Analysis on High Frequency Signal: A Review. *Journal of Advanced Research in Applied Sciences and Engineering Technology*, **59**, 299-317. https://doi.org/10.37934/araset.60.1.299317

[2] Shamsan, Z.A. (2020) Rainfall and Diffraction Modeling for Millimeter-Wave Wireless Fixed Systems. *IEEE Access*, **8**, 212961-212978. https://doi.org/10.1109/access.2020.3040624

[3] Hassija, V., Chamola, V., De, R., Das, S., Chakrabarti, A., Sangwan, K.S., *et al.* (2025) A Survey on Digital Twins: Enabling Technologies, Use Cases, Application, Open Issues, and More. *IEEE Journal of Selected Areas in Sensors*, **2**, 84-107. https://doi.org/10.1109/jsas.2024.3523856

[4] Ayo, A.O., Owolawi, P.A. and Ojo, J.S. (2024) Time Series Forecasting of Rain-Induced Attenuation Using Coupled ARIMA-SARIMA Models for Radio Propagation Applications over Subtropical Locations. *Edelweiss Applied Science and Technology*, **8**, 3100-3128. https://doi.org/10.55214/25768484.v8i6.2661

[5] Sagheer, A. and Kotb, M. (2019) Time Series Forecasting of Petroleum Production Using Deep LSTM Recurrent Networks. *Neurocomputing*, **323**, 203-213. https://doi.org/10.1016/j.neucom.2018.09.082

[6] Matondo, S.B. and Owolawi, P.A. (2025) Impact of Rain Attenuation on Path Loss and Link Budget in 5G mmWave Wireless Propagation under South Africa's Subtropical Climate. *Telecom*, **6**, Article 66. https://doi.org/10.3390/telecom6030066

[7] Ayo, A.O., Owolawi, P.A., Ojo, J.S. and Mpoporo, L.J. (2020) Rain Impairment Model for Satellite Communication Link Design in South Africa Using Neural Network. 2020 2*nd International Multidisciplinary Information Technology and Engineering Con-*

ference (*IMITEC*), Kimberley, 25-27 November 2020, 1-8. https://doi.org/10.1109/imitec50163.2020.9334080

[8] Orsi, X., Hierro, R., Llamedo, P., Alexander, P. and de la Torre, A. (2025) Forecasting Intense Radar Reflectivity Using Machine Learning and Deep Learning Algorithms. *International Journal of Climatology*, **45**, e8919. https://doi.org/10.1002/joc.8919

[9] Dahman, I., Arbogast, P., Jeannin, N. and Benammar, B. (2018) Rain Attenuation Prediction Model for Satellite Communications Based on the Météo-France Ensemble Prediction System Pearp. *Natural Hazards and Earth System Sciences*, **18**, 3327-3341. https://doi.org/10.5194/nhess-18-3327-2018

[10] Hadwan, M., M. Al-Maqaleh, B., N. Al-Badani, F., Ullah Khan, R. and A. Al-Hagery, M. (2022) A Hybrid Neural Network and Box-Jenkins Models for Time Series Forecasting. *Computers, Materials & Continua*, **70**, 4829-4845. https://doi.org/10.32604/cmc.2022.017824

[11] Martínez-Acosta, L., Medrano-Barboza, J.P., López-Ramos, Á., Remolina López, J.F. and López-Lambraño, Á.A. (2020) SARIMA Approach to Generating Synthetic Monthly Rainfall in the Sinú River Watershed in Colombia. *Atmosphere*, **11**, Article 602. https://doi.org/10.3390/atmos11060602

[12] Danandeh Mehr, A., Ghadimi, S., Marttila, H. and Torabi Haghighi, A. (2022) A New Evolutionary Time Series Model for Streamflow Forecasting in Boreal Lake-River Systems. *Theoretical and Applied Climatology*, **148**, 255-268. https://doi.org/10.1007/s00704-022-03939-3

[13] Fatima, S.S.W. and Rahimi, A. (2024) A Review of Time-Series Forecasting Algorithms for Industrial Manufacturing Systems. *Machines*, **12**, Article 380. https://doi.org/10.3390/machines12060380

[14] Kumar, D.S., Thiruvarangan, B.C., Sai Nikhil Reddy, C., Vishnu, A., Devi, A.S. and Kavitha, D. (2022) Analysis and Prediction of Stock Price Using Hybridization of SARIMA and XGBoost. 2022 *International Conference on Communication, Computing and Internet of Things* (*IC3IoT*), Chennai, 10-11 March 2022, 1-4. https://doi.org/10.1109/ic3iot53935.2022.9767868

[15] Woldamanuel, E.M. and Diba, F.D. (2022) Enhanced Adaptive Code Modulation for Rainfall Fade Mitigation in Ethiopia. *EURASIP Journal on Wireless Communications and Networking*, **2022**, Article No. 8. https://doi.org/10.1186/s13638-021-02085-0

[16] Alozie, E., Abdulkarim, A., Abdullahi, I., Usman, A.D., Faruk, N., Olayinka, I.Y., *et al.* (2022) A Review on Rain Signal Attenuation Modeling, Analysis and Validation Techniques: Advances, Challenges and Future Direction. *Sustainability*, **14**, Article 11744. https://doi.org/10.3390/su141811744

[17] Salehin, I., Talha, I.M., Mehedi Hasan, M., Dip, S.T., Saifuzzaman, M. and Moon, N.N. (2020) An Artificial Intelligence Based Rainfall Prediction Using LSTM and Neural Network. 2020 *IEEE International Women in Engineering* (*WIE*) *Conference on Electrical and Computer Engineering* (*WIECON-ECE*), Bhubaneswar, 26-27 December 2020, 5-8. https://doi.org/10.1109/wiecon-ece52138.2020.9398022

[18] Fente, D.N. and Kumar Singh, D. (2018) Weather Forecasting Using Artificial Neural Network. 2018 *Second International Conference on Inventive Communication and Computational Technologies* (*ICICCT*), Coimbatore, 20-21 April 2018, 1757-1761. https://doi.org/10.1109/icicct.2018.8473167

[19] Ma, X., Tao, Z., Wang, Y., Yu, H. and Wang, Y. (2015) Long Short-Term Memory Neural Network for Traffic Speed Prediction Using Remote Microwave Sensor Data. *Transportation Research Part C: Emerging Technologies*, **54**, 187-197. https://doi.org/10.1016/j.trc.2015.03.014

[20] Zeroual, A., Harrou, F., Dairi, A. and Sun, Y. (2020) Deep Learning Methods for Forecasting COVID-19 Time-Series Data: A Comparative Study. *Chaos, Solitons & Fractals*, **140**, Article ID: 110121. https://doi.org/10.1016/j.chaos.2020.110121

[21] Ojo, J.S. and Owolawi, P.A. (2014) Development of One-Minute Rain-Rate and Rain-Attenuation Contour Maps for Satellite Propagation System Planning in a Subtropical Country: South Africa. *Advances in Space Research*, **54**, 1487-1501. https://doi.org/10.1016/j.asr.2014.06.028

[22] Lian, B., Wei, Z., Sun, X., Li, Z. and Zhao, J. (2022) A Review on Rainfall Measurement Based on Commercial Microwave Links in Wireless Cellular Networks. *Sensors*, **22**, Article 4395. https://doi.org/10.3390/s22124395

[23] Zhao, Y., Liu, X., Xian, M. and Gao, T. (2021) Statistical Study of Rainfall Inversion Using the Earth-Space Link at the Ku Band: Optimization and Validation for 1 Year of Data. *IEEE Journal of Selected Topics in Applied Earth Observations and Remote Sensing*, **14**, 9486-9494. https://doi.org/10.1109/jstars.2021.3111336

[24] Christofilakis, V., Tatsis, G., Chronopoulos, S., Sakkas, A., Skrivanos, A., Peppas, K., *et al.* (2020) Earth-to-Earth Microwave Rain Attenuation Measurements: A Survey on the Recent Literature. *Symmetry*, **12**, Article 1440. https://doi.org/10.3390/sym12091440

[25] Su, G.Y., Han, C.Z., Bi, Y.H., Liu, K. and Bao, L. (2020) Monitoring and Analysis of Water Vapor Density Based on Wireless Communication Network in Gothenburg Area. *Journal of Infrared and Millimeter Waves*, **39**, 47-55.

[26] Han, C., Su, G., Bao, L. and Messer, H. (2022) Water Vapor Density Retrieval Studies Using Commercial Millimeter-Wave Links at 38 GHz and E-Band. *Remote Sensing*, **14**, Article 946. https://doi.org/10.3390/rs14040946

[27] Song, K., Liu, X., Gao, T. and Zhang, P. (2021) Estimating Water Vapor Using Signals from Microwave Links Below 25 GHz. *Remote Sensing*, **13**, Article 1409. https://doi.org/10.3390/rs13081409

[28] Ostrometzky, J., Cherkassky, D. and Messer, H. (2015) Accumulated Mixed Precipitation Estimation Using Measurements from Multiple Microwave Links. *Advances in Meteorology*, **2015**, Article ID: 707646. https://doi.org/10.1155/2015/707646

[29] Burnham, K.P. and Anderson, D.R. (2001) Kullback-Leibler Information as a Basis for Strong Inference in Ecological Studies. *Wildlife Research*, **28**, 111-119. https://doi.org/10.1071/wr99107

[30] Cavanaugh, J.E. and Neath, A.A. (2019) The Akaike Information Criterion: Background, Derivation, Properties, Application, Interpretation, and Refinements. *WIREs Computational Statistics*, **11**, e1460. https://doi.org/10.1002/wics.1460

[31] Paul, J.C., Hoque, S. and Rahman, M.M. (2013) Selection of Best ARIMA Model for Fore-Casting Average Daily Share Price Index of Pharmaceutical Companies in Bangladesh: A Case Study on Square Pharmaceutical LTD. *Global Journal of Management and Business Research Finance*, **13**, 14-25.

[32] Houssein, E.H., Mohamed, M., Younis, E.M.G. and Mohamed, W.M. (2025) Artificial Intelligence and Classical Statistical Models for Time Series Forecasting: A Comprehensive Review. *Journal of Big Data*, **12**, Article No. 271. https://doi.org/10.1186/s40537-025-01318-z

[33] Akshay, K.C., Grace, G.H., Gunasekaran, K. and Samikannu, R. (2024) Power Consumption Prediction for Electric Vehicle Charging Stations and Forecasting Income. *Scientific Reports*, **14**, Article No. 6497. https://doi.org/10.1038/s41598-024-56507-2

[34] Matricciani, E. and Riva, C. (2025) Conversion of 10 Min Rain Rate Time Series into 1 Min Time Series: Theory, Experimental Results, and Application in Satellite Com-

munications. *Applied Sciences*, **15**, Article 743. https://doi.org/10.3390/app15020743

[35] Ojo, J.S. and Owolawi, P.A. (2015) Application of Synthetic Storm Technique for Diurnal and Seasonal Variation of Slant Path Ka-Band Rain Attenuation Time Series over a Subtropical Location in South Africa. *International Journal of Antennas and Propagation*, **2015**, Article ID: 474397. https://doi.org/10.1155/2015/474397

[36] Afolayan, B.O., Afullo, T.J. and Alonge, A. (2018) Subtropical Rain Attenuation Statistics on 12.6 GHz Ku-Band Satellite Link Using Synthetic Storm Technique. *SAIEE Africa Research Journal*, **109**, 230-236. https://doi.org/10.23919/saiee.2018.8538336

[37] Adjei-Frimpong, B. and Csurgai-Horváth, L. (2018) Using Radio Wave Satellite Propagation Measurements for Rain Intensity Estimation. *Infocommunications journal*, **10**, 2-8. https://doi.org/10.36244/icj.2018.3.1

[38] Shatanawi, K., Rahbeh, M. and Shatanawi, M. (2013) Characterizing, Monitoring and Forecasting of Drought in Jordan River Basin. *Journal of Water Resource and Protection*, **5**, 1192-1202. https://doi.org/10.4236/jwarp.2013.512127

[39] Bari, S.H., Rahman, M., Hussain, M. and Ray, S. (2015) Forecasting Monthly Precipitation in Sylhet City Using ARIMA Model. *Civil and Environmental Research*, **7**, 69-77.

[40] Farsi, M., Hosahalli, D., Manjunatha, B.R., Gad, I., Atlam, E., Ahmed, A., *et al.* (2021) Parallel Genetic Algorithms for Optimizing the SARIMA Model for Better Forecasting of the NCDC Weather Data. *Alexandria Engineering Journal*, **60**, 1299-1316. https://doi.org/10.1016/j.aej.2020.10.052

[41] Kokilavani, S., Pangayarselvi, R., Ramanathan, S.P., Dheebakaran, G., Sathyamoorthy, N.K., Maragatham, N., *et al.* (2020) SARIMA Modelling and Forecasting of Monthly Rainfall Patterns for Coimbatore, Tamil Nadu, India. *Current Journal of Applied Science and Technology*, **39**, 69-76. https://doi.org/10.9734/cjast/2020/v39i830594

[42] Usmani, U.A., Abdul Aziz, I., Jaafar, J. and Watada, J. (2024) Deep Learning for Anomaly Detection in Time-Series Data: An Analysis of Techniques, Review of Applications, and Guidelines for Future Research. *IEEE Access*, **12**, 174564-174590. https://doi.org/10.1109/access.2024.3495819

[43] Samad, M.A., Diba, F.D. and Choi, D.-Y. (2021) A Survey of Rain Attenuation Prediction Models for Terrestrial Links-Current Research Challenges and State-of-the-Art. *Sensors*, **21**, Article 1207. https://doi.org/10.3390/s21041207

[44] Mienye, I.D., Swart, T.G. and Obaido, G. (2024) Recurrent Neural Networks: A Comprehensive Review of Architectures, Variants, and Applications. *Information*, **15**, Article 517. https://doi.org/10.3390/info15090517

[45] Shaqiri, F. (2024) Applications of Time Series Forecasting Models, Decomposition Methods, Non-Parametric Regression Methods, and Artificial Neural Networks. Fraunhofer Verlag.

[46] Leiprecht, S., Behrens, F., Faber, T. and Finkenrath, M. (2021) A Comprehensive Thermal Load Forecasting Analysis Based on Machine Learning Algorithms. *Energy Reports*, **7**, 319-326. https://doi.org/10.1016/j.egyr.2021.08.140

[47] Song, X., Liu, Y., Xue, L., Wang, J., Zhang, J., Wang, J., *et al.* (2020) Time-series Well Performance Prediction Based on Long Short-Term Memory (LSTM) Neural Network Model. *Journal of Petroleum Science and Engineering*, **186**, Article ID: 106682. https://doi.org/10.1016/j.petrol.2019.106682

[48] Elsaraiti, M. and Merabet, A. (2021) A Comparative Analysis of the ARIMA and LSTM Predictive Models and Their Effectiveness for Predicting Wind Speed. *Energies*, **14**, Article 6782. https://doi.org/10.3390/en14206782

[49] Karim, F.K., Khafaga, D.S., El-kenawy, E.M., Eid, M.M., Ibrahim, A., Abualigah, L., *et al.* (2024) Optimized LSTM for Accurate Smart Grid Stability Prediction Using a Novel Optimization Algorithm. *Frontiers in Energy Research*, **12**, Article 1399464. https://doi.org/10.3389/fenrg.2024.1399464

[50] Reyad, M., Sarhan, A.M. and Arafa, M. (2023) A Modified Adam Algorithm for Deep Neural Network Optimization. *Neural Computing and Applications*, **35**, 17095-17112. https://doi.org/10.1007/s00521-023-08568-z

[51] Balawi, M. and Tenekeci, G. (2024) Time Series Traffic Collision Analysis of London Hotspots: Patterns, Predictions and Prevention Strategies. *Heliyon*, **10**, e25710. https://doi.org/10.1016/j.heliyon.2024.e25710

[52] Ebhuoma, O., Gebreslasie, M. and Magubane, L. (2018) A Seasonal Autoregressive Integrated Moving Average (SARIMA) Forecasting Model to Predict Monthly Malaria Cases in Kwazulu-Natal, South Africa. *South African Medical Journal*, **108**, 573-578. https://doi.org/10.7196/samj.2018.v108i7.12885

[53] Wilson, G.T. (2016) Time Series Analysis: Forecasting and Control, 5th Edition, by George E. P. Box, Gwilym M. Jenkins, Gregory C. Reinsel and Greta M. Ljung, 2015. Published by John Wiley and Sons Inc., Hoboken, New Jersey, pp. 712. ISBN: 978-1-118-67502-1. *Journal of Time Series Analysis*, **37**, 709-711. https://doi.org/10.1111/jtsa.12194

[54] Nwokike, C.C., Offorha, B.C., Obubu, M., Ugoala, C.B. and Ukomah, H.I. (2020) Comparing SANN and SARIMA for Forecasting Frequency of Monthly Rainfall in Umuahia. *Scientific African*, **10**, e00621. https://doi.org/10.1016/j.sciaf.2020.e00621